RSC Advances

ROYAL SOCIETY OF CHEMISTRY

PAPER

View Article Online
View Journal | View Issue

Cite this: *RSC Adv.*, 2025, **15**, 48678

One-step hydrothermal preparation of WO_3–carbon felt for electrolytic recovery of copper from PCB wastewater

Jingtao Sun,†[a] Dengxiang Fan,†[a] Han Zhang,[a] Yunlong Dong,[b] Liu Jiang,[c] Guobin Li,[c] Miaomiao Yang,[a] Weiwei Xi,[a] Rongfang Yuan,[a] Beihai Zhou,[a] Huilun Chen[a] and Shuai Luo *[a]

Recovering copper from printed circuit board (PCB) wastewater remains challenging due to complex coexisting ions and high organic content. Here, a WO_3–carbon felt electrode was fabricated through a one-step hydrothermal method followed by binder-free spray coating, producing a sea-urchin/plate-like WO_3 morphology with strong adhesion and high electrochemical activity. The WO_3–carbon felt electrode achieved a 70.1% copper removal efficiency at 1.2 V, outperforming unmodified carbon felt due to enhanced surface area, reduced charge-transfer resistance, and improved electrocatalytic kinetics. Orthogonal optimization identified voltage and pH as the dominant factors affecting performance. The electrode also maintained stable efficiency in actual PCB wastewater with high COD, demonstrating strong anti-interference capability. Cost analysis demonstrated that the WO_3–carbon felt electrode exhibited a markedly lower unit-area cost (24.8 USD m^{-2}) than graphite or Sn–Sb/Ti electrodes, confirming its economic feasibility. This study highlights a facile, scalable strategy for developing oxide–carbon composite electrodes with promising application potential in metal recovery and industrial wastewater treatment.

Received 30th September 2025
Accepted 20th November 2025

DOI: 10.1039/d5ra07199b

rsc.li/rsc-advances

1 Introduction

In the era of the rapidly expanding smart economy, the integration of digitalization and automation technologies has significantly accelerated the growth of the electrical and electronic equipment (EEE) manufacturing sector. This development, however, has intensified the demand for critical and scarce metal resources. Wasted electrical and electronic equipment (WEEE), also known as electronic waste (E-waste), has emerged as one of the fastest-growing global solid waste streams. This surge is driven by the rapid pace of technological innovation, as well as evolving social and economic dynamics.[1] According to the Global E-waste Monitor 2020, more than 50 million tons of E-waste were generated worldwide in 2019.[2] Among all E-waste components, PCB is an essential element of all E-waste components. Structurally, PCBs consist of copper-clad laminates made from glass fiber reinforced epoxy resin and contain multiple metallic components. In addition to copper (Cu), these include nickel (Ni), lead (Pb),[3] tin (Sn), gold (Au), palladium (Pd), silver (Ag), cobalt (Co), and trace amounts of cadmium (Cd) and mercury (Hg).[4] These metals originate from solder alloys, circuit plating, and electronic connectors, posing both environmental hazards and opportunities for resource recovery.[5] The widespread adoption of electronic products in the 21st century has led to a dramatic increase in PCB production, exacerbating the environmental footprint of electronic manufacturing.[6,7] Traditionally, the recovery of copper from E-waste has relied on complex, multi-stage pyrometallurgical or hydrometallurgical processes.[8,9] These are typically followed by downstream techniques such as chemical precipitation, ion exchange, adsorption, solvent extraction and electrochemical deposition to achieve metal separation and purification.[10,11] However, due to the heterogeneous nature of E-waste and regional limitations in resources and infrastructure, global implementation of unified strategies for E-waste management is challenging. Therefore, the development of sustainable urban mining systems for copper recovery has increasingly focused on designing efficient, cost-effective, and environmentally benign technologies.[12]

Electrochemical technology has proven to be an effective method for pollutant removal and heavy metal recovery from wastewater. With advantages including low cost, operation facilitation, and high pollutant removal efficiency, the electrochemical technology has been widely adopted for large-scale

[a]*Beijing Key Laboratory of Resource-Oriented Treatment of Industrial Pollutants, School of Energy and Environmental Engineering, University of Science and Technology Beijing, Beijing 100083, China. E-mail: shuailuo@ustb.edu.cn*

[b]*Choate Rosemary Hall, 333 Christian St, Wallingford, CT 06492, USA*

[c]*Guangdong Qinhua Smart Environment Technology Co., Ltd, Dongguan 523808, China*

† The two authors contribute equally to this work.

applications with high efficiency to recover the metal.[13–15] Electrochemical processes encompassed a range of techniques, including electrolysis, electrooxidation, electroreduction, electrocoagulation, capacitive deionization and bioelectrochemical systems.[16] Electrolysis, in particular, utilizes electrochemical principles for sustainable waste treatment and environmental remediation, offering a promising pathway for the recovery and reuse of energy and resources. Numerous studies have demonstrated the successful application of electrolysis in recovering heavy metals from industrial wastewater.[14,17,18] In parallel, advances in electronic sensor technologies have enabled rapid detection of metal ions in E-waste leachates,[19] which complement electrochemical recovery strategies by improving process monitoring and control. However, there was still limited research about PCB wastewater. Electrolysis has been shown to effectively recover significant amounts of heavy metals, particularly copper, from PCB wastewater, with both environmental and efficiency advantages.[20] While electrochemical methods for heavy metal recovery have been extensively studied in the context of industrial wastewater, limited research has specifically focused on treating PCB wastewater using these technologies.[21–23] Additionally, there is a lack of comprehensive studies on the influence of operational parameters—such as applied voltage, pH, and reactor design—on the efficiency of electrochemical treatment processes.

The choice of electrode material plays a crucial role in the performance of electrochemical systems, as it directly affects electron transfer efficiency, surface area, and overall reaction kinetics.[24–26] Tungsten trioxide (WO_3) is a promising electroactive material, widely used for electrode modification in sensors, supercapacitors, and other electrochemical devices due to its enhanced capacitance and electroadsorption properties.[27–29] Thus, WO_3 is promising to be applied to increase the treatment efficiency of the industrial wastewater and the metal recovery.

In this study, we focus on developing a simple yet robust WO_3–carbon felt composite electrode for electrochemical copper recovery from printed circuit board (PCB) wastewater. While numerous studies have reported metal oxide–carbon composite electrodes, the present work introduces distinctive advances in both fabrication and application. Specifically, (i) a one-step, low-temperature hydrothermal synthesis was employed to directly generate sea-urchin/plate-like WO_3 nanostructures on commercial carbon felt, avoiding complex multistep or binder-assisted processes; (ii) a binder-free spray-coating procedure was used to ensure uniform WO_3 coverage while preserving the inherent porosity and conductivity of the felt substrate; and (iii) the electrode's performance was systematically evaluated in both simulated and actual PCB wastewater, characterized by high chemical oxygen demand (COD) and coexisting ions—conditions rarely addressed in previous studies on WO_3-based electrodes. These combined features highlight the practical novelty of this work, demonstrating a facile synthesis route, durable electrode architecture, and reliable performance under realistic industrial wastewater conditions, thereby offering new insights into the design of oxide–carbon composite electrodes for metal recovery applications.

2 Experiments and methods

2.1 Experimental drugs and instruments

2.1.1 Experimental setup. The electrochemical system employed in this study was illustrated in Fig. 1. It consisted of a sealed electrolytic cell, a DC-regulated power supply, a magnetic stirrer, and electrode rods. The electrolytic cell was custom-fabricated, featuring a polytetrafluoroethylene (PTFE) lid equipped with three 6.5 mm electrode ports and two 3.2 mm gas vents. The cell body was constructed from borosilicate glass with an approximate volume of 500 mL.

2.1.2 Experimental reagents. All reagents used in this study were of analytical reagent (AR) grade and used without further purification. Sulfuric acid (H_2SO_4), nitric acid (HNO_3), hydrochloric acid (HCl), oxalic acid ($H_2C_2O_4$), anhydrous ethanol (C_2H_5OH), sodium hydroxide (NaOH), copper sulfate pentahydrate ($CuSO_4 \cdot 5H_2O$), acetone (C_3H_6O), isopropanol (C_3H_8O) and glucose ($C_6H_{12}O_6$) were all purchased from China National Pharmaceutical Group. Sodium tungstate (Na_2WO_4) was supplied by McLean Biochemical Technology Co. Copper standard solution ($Cu(NO_3)_2$) was provided by Beijing Tianwei Teda Technology Co.

2.1.3 Laboratory instruments. pH values were measured with a pH meter (Starter3C, Ohaus Instruments). Morphological and elemental characterizations were performed by scanning electron microscopy (SEM, XL30 ESEM FEG, FEI Company) and X-ray photoelectron spectroscopy (XPS, ESCA-LAB 250, Thermo Fisher Scientific). Phase identification was conducted using X-ray diffraction (XRD, D8 ADVANCE, Bruker Corporation, Germany). The concentration of metal ions was determined by inductively coupled plasma optical emission spectrometry (ICP-OES, OPTIMA 8300, PerkinElmer). Electrochemical experiments were performed using an electrochemical workstation (CHI660E, Chenhua Instrument Co., Ltd., Shanghai) in combination with a DC power supply (MS1510DS, Maisheng Power Technology Co., Ltd.). A data acquisition system (34970A, Keysight Technologies, USA) was used for real-time monitoring and data collection.

2.2 Experimental methods

2.2.1 Preparation of WO_3–carbon felt electrode. Carbon felts (5×10 cm^2) were first pre-cut and sequentially cleaned with ultrapure water and anhydrous ethanol, followed by drying in an oven at 50 °C. The dried carbon felts were then immersed in concentrated nitric acid (68% w/w HNO_3) and placed in a fume hood for 24 hours. After acid treatment, the felts were rinsed thoroughly with anhydrous ethanol and ultrapure water to remove surface impurities and subsequently dried for further use.

WO_3–carbon felt electrode was later synthesized under the specific procedures. WO_3 powder and WO_3–carbon felt electrodes were synthesized *via* a one-step hydrothermal method. Sodium tungstate (Na_2WO_4) served as the tungsten source,

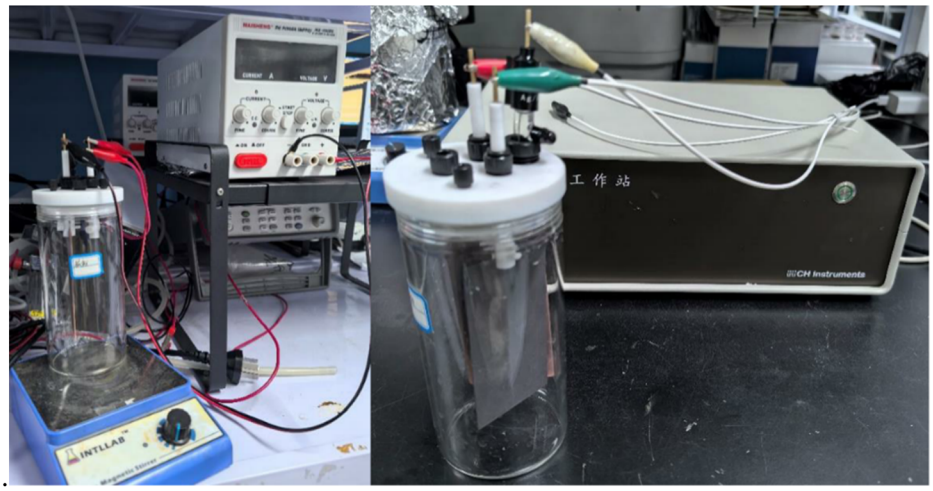

Fig. 1 Experimental device diagram.

while concentrated hydrochloric acid (36–38% HCl) and oxalic acid ($C_2H_2O_4 \cdot 2H_2O$) acted as the proton donor and dispersing agent, respectively. Specifically, 1.45 g of Na_2WO_4 was dissolved in 40 mL of ultrapure water (resulting in a 0.12 M solution). Then, 4 mL of concentrated HCl was slowly added under stirring to form a homogeneous white-yellow solution. Subsequently, 1 g of oxalic acid crystals was added, and the final mixture was stirred continuously until the solution turned colorless, indicating that the solution was fully prepared. The solution was transferred to a 200 mL Teflon-lined stainless-steel autoclave, subjected to hydrothermal treatment at 200 °C for 12 hours, and then cooled naturally to room temperature.

After the reaction, the resulting yellow suspension was stirred and transferred to a centrifuge tube. The mixture was centrifuged at 8000 rpm for 5 minutes. The precipitate was collected, washed successively with ultrapure water and anhydrous ethanol. Finally the precipitate was finally dried at 50 °C to obtain the WO_3 powder. During the synthesis, sodium tungstate in aqueous solution generated tungstate ions to be mixed with protons and react to form metatungstic acid (H_2WO_4) under acidic conditions. Upon hydrothermal treatment at elevated temperature and pressure, WO_3 nanorods with a sea-urchin-like three-dimensional structure were formed. The solution pH increased gradually during the reaction, which was predicted to inhibit further hydrolysis of sodium tungstate. Once the pH exceeded 5, the reaction would cease. The presence of oxalic acid provided a slow and sustained release of protons, which stabilized the pH and ensured continuous formation of WO_3. A schematic diagram of the hydrothermal synthesis process was presented in Fig. 2. The overall reaction mechanism can be summarized by equations below.

$$Na_2WO_4 + 2HCl + H_2O = H_2WO_4 \cdot nH_2O + 2NaCl$$

$$H_2WO_4 \cdot H_2O \rightarrow WO_3 + (n + 1)H_2O$$

A portion of the synthesized WO_3 powder was dispersed in a 1 : 1 (v/v) mixture of acetone and isopropanol. The suspension was stirred for 5 minutes and then subjected to ultrasonic treatment for 10 minutes to ensure thorough dispersion of the WO_3 particles. The resulting homogeneous suspension was uniformly sprayed onto the pretreated carbon felt electrodes using a spray gun. Finally, the coated electrodes were dried in an oven at 60 °C to obtain the WO_3–carbon felt electrodes.

2.2.2 Preparation of other electrode materials. Carbon felt electrode was purchased by large-size carbon felts from the market, and the size was cut into 50 × 100 mm. PAN-based

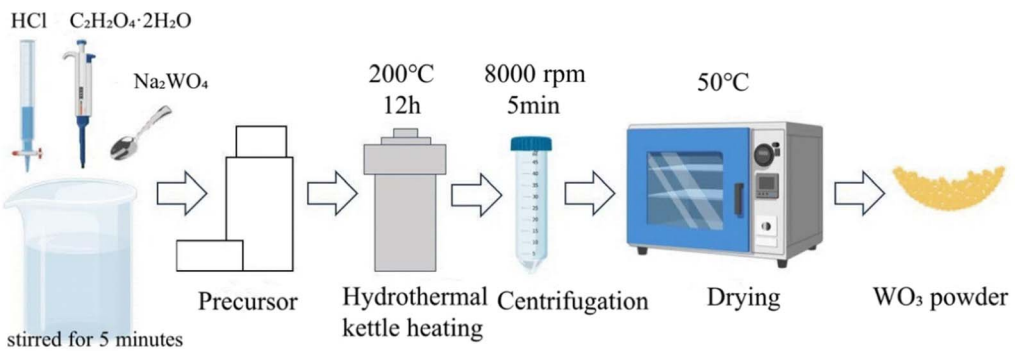

Fig. 2 Schematic diagram of the WO_3 powder preparation process by the hydrothermal method.

carbon fiber felts was prepared with the following properties including density of 0.12–0.13 g cm^{-3}, carbon content of 93–99.9%, porosity of 90%, moisture absorption of 1.0% (using temperature requirements of air 350 °C, vacuum 1800 °C, inert gas 2650 °C). Pre-treatment was required for normal use. Graphite plate electrode was prepared from the commercially available graphite plate electrode, with the properties including size 50 × 100 × 1 mm, bulk density 1.85 g cm^{-3}, resistivity of about 8–10 × 10^{-6} Ω m, thermal conductivity 139.2 W m^{-1}, compressive strength of 85 MPa, porosity ≤13%, carbon content of 99.99%, bulk density of 1.86. Tin–antimony–titanium electrode was prepared by selecting titanium plate size of 50 × 100 × 1 mm, with the properties including moisture absorption 1.0% (using temperature requires air 350 °C, vacuum 1800 °C, inert gas 2650 °C). Tin–antimony–titanium electrode was prepared by the size of the selected titanium plate was 50 × 100 × 1 mm, and the amount of metal used was set at 10 g m^{-2} for tin and 10 g m^{-2} for antimony, with the tin and antimony modified onto the surface of the titanium plate by the method of repeated discharging-sandblasting-acid washing-fluorine coating under the temperature at 500 °C.

2.2.3 Characterization of WO_3–carbon felt electrode. The surface morphology and microstructure of the WO_3–carbon felt electrode were examined using scanning electron microscopy (SEM). The crystal structure was analyzed by X-ray diffraction (XRD), while X-ray photoelectron spectroscopy (XPS) was employed to investigate the elemental composition and chemical valence states. Electrochemical performance was evaluated using a CHI660E electrochemical workstation.

2.2.4 Analytical methods and evaluation indicators. Wastewater samples and those collected during the experimental process were first subjected to microwave digestion as a pretreatment step. The resulting digested solutions were then analyzed using inductively coupled plasma optical emission spectrometry (ICP-OES) to quantify the copper ion concentration. The copper removal efficiency was calculated based on the measured concentrations using the following eqn (1):

$$\eta = \frac{c_0 - c_t}{c_0} \times 100\% \quad (1)$$

where: η represents removal efficiency of Cu^{2+}; c_0 represents the initial concentration of Cu^{2+} (g L^{-1}); c_t represents Cu^{2+} concentration in the sample at reaction time t (g L^{-1}).

The important water quality parameters were of the samples were all tested, and the parameters included chemical oxygen demand (COD), pH, and ammonium nitrogen (NH_4^+–N). The value of COD was determined using the rapid digestion-spectrophotometric method, with specific steps detailed in Text S1. The measurement of ammonia nitrogen was based on HJ 195-2023 using gas phase molecular absorption spectroscopy. The pH value was measured using the glass electrode method.

2.2.5 Electrochemical property measurement. Current efficiency reflects the effectiveness of energy utilization during electrolysis and serves as an important indicator of electrode performance. It was primarily evaluated based on the amount of copper recovered at the end of the electrolysis process. The actual mass of recovered copper was compared with the theoretical recovery calculated based on Faraday's law, using the following eqn (2):

$$n = \frac{\Delta m}{CIt} \times 100\% \quad (2)$$

where n represents cathodic current efficiency (%); Δm represents mass of copper deposited on the cathode after electrolysis (g); C represents electrochemical equivalent of copper (1.186 g A^{-1} h^{-1}); I represents electrolytic current during the reaction (A); t represents electrolysis time (h).

2.2.6 Study on the electrolytic treatment of copper in PCB wastewater. The experimental process utilized simulated PCB wastewater, and then used actual PCB wastewater obtained from a PCB production plant in Guangdong. This wastewater was discharged during the PCB production process. After conducting several quality tests on the water, a set of common water quality parameters were derived, and the results were shown in Table 1. The detailed formulation for simulating copper-containing wastewater is shown in Text S2.

The system performance and electrolytic treatment was evaluated for the copper removal and PCB wastewater. The electrochemical reaction system was established by introducing 400 mL of simulated PCB wastewater into a sealed electrolysis cell. A two-electrode configuration was employed, with a DC power supply (MS1510DS) providing a range of applied voltages. A graphite plate served as the anode, while the cathode materials included two WO_3–carbon felt electrodes synthesized *via* the hydrothermal method, as well as an unmodified carbon felt electrode for comparison. All electrodes were mounted within the sealed electrolysis cell and immersed in the simulated wastewater. To ensure uniformity of the solution, continuous stirring was maintained using an electromagnetic stirrer throughout the electrolysis process. Electrolysis was performed under varying operational parameters—including NaOH dosage, applied voltage, and electrolysis duration—according to a systematic experimental design. Post-electrolysis, both the treated and untreated wastewater samples were diluted 50-fold, and copper ion concentrations were quantified using ICP-OES. To determine the optimal operational conditions influencing copper removal, an orthogonal experimental design was applied. The performance of the WO_3–carbon felt electrodes was evaluated in comparison with the unmodified carbon felt electrode and commonly used commercial electrodes such as graphite plate and tin–antimony–carbon electrodes. Additionally, repeated electrolysis cycles were conducted on the hydrothermally synthesized WO_3–carbon felt electrodes to assess their reusability and long-term electrochemical stability.

Table 1 The concentration of several common pollutant indicators in the actual PCB wastewater of a PCB factory in Guangdong

Contamination index	Cu (mg L^{-1})	pH	COD (mg L^{-1})	NH_4^+–N (mg L^{-1})
	5000	0.70	1000	20

Table 2 Factors and levels setting of orthogonal experiment

	A	*B*	*C*
Factor	NaOH dosage (g L^{-1})	Applied voltage (V)	Electrolysis time (h)
1	0	2.0	3
2	3	2.5	4
3	6	3.0	5
4	9	3.5	6

A three-factor, four-level orthogonal experimental design was employed to systematically investigate the influence of key operating parameters on the removal efficiency of copper from PCB wastewater using the synthesized WO_3–carbon felt electrodes. The three factors considered in this study were NaOH dosage (g L^{-1}), applied voltage (V), and electrolysis time (h). Each factor was studied at four levels, as detailed in Table 2, indicating the variable ranges for each experimental condition. This orthogonal design facilitated the identification of optimal process parameters and gave the direction for the best parameter organization, while minimizing the number of experimental runs required (Table 2)

3 Results and discussion

3.1 Optimization of hydrothermal synthesis conditions

The electrochemical performance of WO_3–carbon felt electrodes was significantly influenced by the amount of WO_3 loading. To investigate this effect, various amounts of WO_3 powder (50 mg, 150 mg, 250 mg, and 350 mg) were dispersed in a 1 : 1 (v/v) acetone–isopropanol mixture containing 5 mL of acetone. The suspensions were stirred for 5 min and ultrasonicated for 10 min to ensure complete dispersion. The resulting homogeneous solutions were uniformly sprayed onto pretreated carbon felt electrodes to achieve WO_3 loadings of 1 mg cm^{-2}, 3 mg cm^{-2}, 5 mg cm^{-2}, and 7 mg cm^{-2}, respectively. The coated electrodes were then dried in an oven at 60 °C for future use.

As shown in Fig. 3, the electrolysis was conducted under a constant applied voltage of 3.0 V for a duration of 5 h using simulated PCB wastewater. Samples were collected at the end of the electrolysis (5 h) to determine the Cu^{2+} removal efficiency. The results revealed a parabolic trend in copper removal efficiency with increasing WO_3 loading. As the WO_3 loading increased from 1 mg cm^{-2} to 7 mg cm^{-2}, the Cu removal rate initially increased and then declined, with removal efficiencies of 39.2%, 43.1%, 52.8%, and 48.9%, respectively. In comparison, the bare carbon felt electrode exhibited a significantly lower Cu removal efficiency of only 28.8%.

The optimal performance was achieved at a WO_3 loading of 5 mg cm^{-2}, where the Cu removal rate reached a maximum of 63.1%. The second highest removal efficiency was observed at 3 mg cm^{-2}, followed by 7 mg cm^{-2}, with the poorest performance at 1 mg cm^{-2}. These results demonstrate that moderate WO_3 loading can effectively enhance the electrochemical performance of carbon felt electrodes. However, excessive WO_3 loading (*e.g.*, 7 mg cm^{-2}) led to a decline in performance, likely due to particle agglomeration, which reduces the effective surface area and the number of available active sites. Additionally, excess WO_3 may block the porous structure of the carbon felt, hindering electrolyte permeability and reducing the contact between Cu^{2+} ions and active sites during electrolysis.

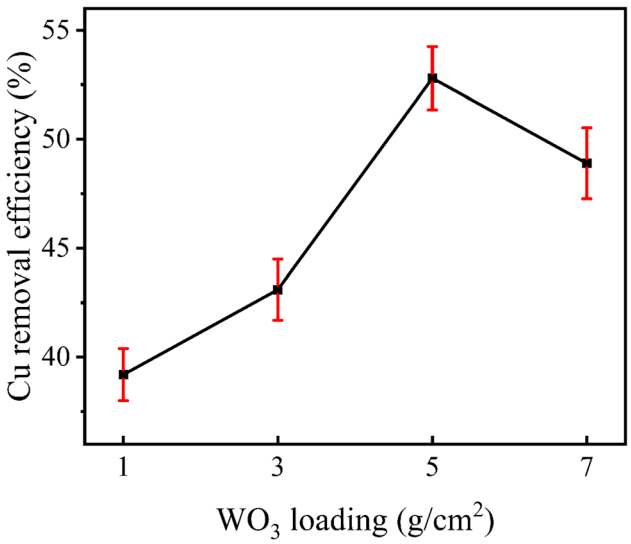

Fig. 3 Effect of WO_3–carbon felt electrode on the removal of Cu from wastewater under different WO_3 loading.

In summary, the WO_3–carbon felt electrode outperformed the unmodified carbon felt in terms of Cu^{2+} removal. However, an optimal WO_3 loading was crucial for maximizing electrochemical efficiency. Based on the experimental results, the optimal WO_3 loading in this study was determined to be 5 mg cm^{-2}.

3.2 Characterization of WO_3–carbon felt electrode

3.2.1 Material characterization. To investigate the surface morphology and microstructure of the prepared samples, SEM analysis was performed on the WO_3 powder and the WO_3–carbon felt electrode synthesized *via* the hydrothermal method. Fig. 4 presents SEM images of the WO_3 powder, the hydrothermal WO_3–carbon felt electrode, and the pristine carbon felt.

Fig. 4(a–c) presents the WO_3 powder at magnifications corresponding to scale bars of 1 μm, 400 nm, and 200 nm, respectively. At 1 μm scale, the particles exhibited a plate-like morphology with uniform distribution. Higher magnification images (400 nm and 200 nm) revealed that the particles possess a plate-like structure with lateral dimensions of approximately 200–800 nm and a thickness ranging from 40 to 100 nm. The presence of nanosheets and layered structures on the particle surfaces enhanced the specific surface area, which was beneficial for promoting electrochemical catalytic activity. Fig. 4(d–f) presented the SEM images of the WO_3–carbon felt electrode at 2 μm, 1 μm, and 400 nm scales. The carbon fibers had diameters of approximately 10–15 μm, and WO_3 particles were uniformly distributed on their surfaces. This uniform coverage indicates that the spray-coating method effectively deposits WO_3 onto the

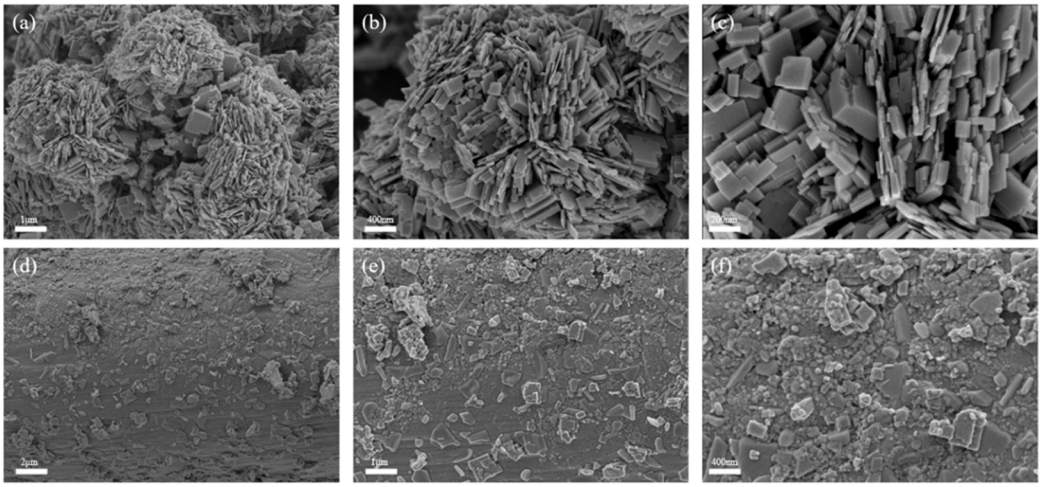

Fig. 4 SEM images of (a–c) WO_3 powder and (d–f) WO_3–carbon felt electrode from low to high magnification.

carbon felt without forming large agglomerates, suggesting that a loading of 5 mg cm^{-2} was optimal and did not exceed the threshold for particle aggregation. At higher magnifications (1 μm and 400 nm), the WO_3 maintains its plate-like morphology consistent with that of the pristine WO_3 powder, indicating that the spraying process did not alter the particle structure significantly. Moreover, the numerous inter-particle gaps observed provide channels for electrolyte penetration and increase the overall specific surface area of the WO_3–carbon felt, thereby enhancing its electrochemical performance.

3.2.1.1 XRD. Fig. S1 presents the XRD patterns of the hydrothermally synthesized WO_3 powder and the WO_3–carbon felt electrode. As shown in Fig. S1(a), the WO_3 powder exhibited characteristic diffraction peaks at 2θ values of 23.2°, 23.6°, 24.4°, 26.6°, 28.7°, 33.4°, 34.2°, 41.9°, 47.3°, 49.9°, and 56.0°, corresponding to the (002), (020), (200), (112), (022), (202), (222), (004), (140), and (420) crystal planes of WO_3, respectively. All peaks match well with the standard diffraction data from the JCPDS card no. 85-2459, with no detectable impurity peaks, indicating that the synthesized WO_3 powder possesses high purity and crystallinity. Fig. S1(b) shows the XRD pattern of the WO_3–carbon felt electrode prepared *via* the hydrothermal method. The observed peaks at 2θ values of 23.0°, 23.5°, 24.3°, 26.5°, 28.9°, 33.1°, 34.1°, 41.8°, 48.2°, 49.9°, and 55.9° correspond to the same WO_3 crystal planes as the powder sample, confirming the presence of crystalline WO_3 on the carbon felt. The diffraction peaks align well with the JCPDS card no. 71-2141, and no additional impurity peaks were detected. These results verify the successful deposition of highly crystalline WO_3 on the carbon felt *via* the hydrothermal synthesis.

3.2.1.2 XPS. To further confirm the chemical composition and valence states of the samples, XPS analysis was conducted on both the hydrothermally synthesized WO_3 powder and the WO_3–carbon felt electrode. The acquired spectra were processed using peak-fitting software XPSPEAK41, concerning the *Chemical Element Binding Energy Handbook* for accurate peak assignment. The resulting XPS spectra of the two materials are presented in Fig. S2.

The characteristic energy loss peaks of tungsten metal typically appear near 37 eV, while those of WO_3 are observed around 42 eV. As shown in Fig. S2(a), the XPS survey spectrum of the WO_3 powder sample reveals the presence of W, C, and O elements without any detectable impurities. The main C 1s peak appears at 284.38 eV, which is corrected to 284.80 eV. Due to the high oxygen content in the pure WO_3 powder, the C=O peak is relatively weak.

The high-resolution W 4f spectrum of the WO_3 powder (Fig. S2(c)) shows peaks at binding energies of 35.39 eV (W $4f_{7/2}$, 60.47%) and 37.53 eV (W $4f_{5/2}$, 36.65%), indicating that tungsten exists predominantly in the hexavalent state (W^{6+}).[30] Additionally, a smaller peak at 41.45 eV (2.88%) corresponds to the characteristic energy loss feature of WO_3, further confirming the W^{6+} valence state.[31] These results demonstrate that the WO_3 powder synthesized *via* the hydrothermal method is of high purity with hexavalent tungsten, effectively excluding the presence of pentavalent or tetravalent tungsten species.[32] Similarly, the W 4f spectrum of the WO_3–carbon felt electrode (Fig. S2(f)) displays binding energies of 35.47 eV (W $4f_{7/2}$, 60.53%), 37.60 eV (W $4f_{5/2}$, 30.92%), and 41.52 eV (loss feature, 2.55%), consistent with those of the pure WO_3 powder. Within experimental error, these results indicated that no valence state changes occur during the process of dispersing WO_3 in the acetone–isopropanol mixture, spray-coating onto carbon felt, and drying. This confirms the chemical stability of WO_3 throughout electrode preparation.

3.2.2 Characterization of electrochemical properties

3.2.2.1 Cyclic voltammetry (CV). To evaluate the electrochemical properties of the WO_3–carbon felt electrode synthesized *via* the hydrothermal method and compare it with those of the pristine carbon felt electrode, cyclic voltammetry tests were performed on both materials. The measurements were conducted using a three-electrode electrochemical workstation system, where the WO_3–carbon felt and ordinary carbon felt served as the working electrodes, a platinum electrode as the counter electrode, and an Ag/AgCl electrode as the reference electrode. The electrolyte was 1 M H_2SO_4, and the potential was scanned between −0.6 V

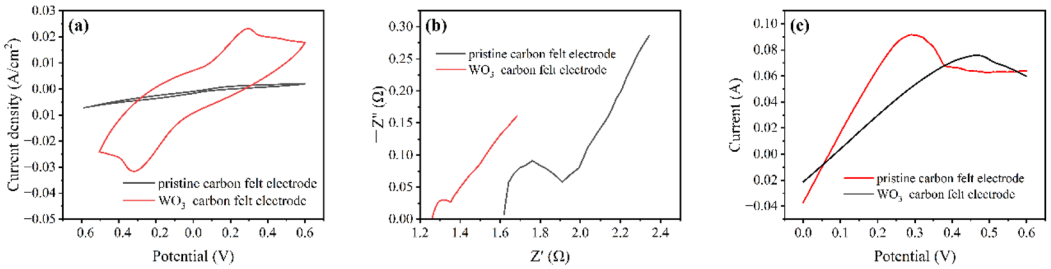

Fig. 5 Electrochemical test results including (a) CV curves, (b) Nernst impedance diagram and (c) LSV test diagram of the pristine carbon felt electrode and the WO_3–carbon felt electrode.

and 0.6 V at a fixed scan rate of 5 mV s^{-1}. As shown in Fig. 5(a), the CV curves of the hydrothermally prepared WO_3–carbon felt electrode exhibit two distinct redox peaks, indicating reversible redox reactions between WO_3 and the electrolyte. This suggests that tungsten species on the carbon felt undergo valence state changes, which were highly sensitive to charge transfer processes.

Compared to the CV curves of the pristine carbon felt electrode, the enclosed area of the WO_3–carbon felt electrode's CV curve was significantly larger, demonstrating a higher capacitance and enhanced electron transfer efficiency. The specific capacitance of the WO_3-modified electrode reached 1.54 F cm^{-2}, exceeding that of the pristine carbon felt electrode (0.0731 F cm^{-2}) by more than 20 times. This improvement can be attributed to the large specific surface area and superior adsorption capacity of WO_3, which increases the number of reactive sites on the composite electrode.

Moreover, the quasi-symmetrical shape of the CV curves for the WO_3–carbon felt electrode indicates excellent capacitive behavior, including pseudocapacitance characteristics, further confirming the enhanced electrochemical performance imparted by the hydrothermal modification.

3.2.2.2 EIS. To evaluate the differences in electrical conductivity of WO_3–carbon felt electrodes prepared *via* the hydrothermal method, electrochemical impedance spectroscopy (EIS) measurements were performed. These tests provided insight into the resistive properties of the electrodes. EIS measurements were conducted in 1 M H_2SO_4 solution, using the hydrothermally prepared WO_3–carbon felt electrode, pristine carbon felt electrode, and graphite electrode as the working electrodes, with a platinum electrode as the counter electrode and Ag/AgCl as the reference electrode.

The equivalent circuit models used to fit the EIS data are shown in Fig. S3. Constant-phase elements (CPE) were employed to better represent the non-ideal capacitive behavior of the porous WO_3-carbon felt electrode. The fitting results, including the resistance values for different electrodes, are summarized in Table 3 and Fig. 5(b).

By analyzing the fitted parameters in Table 3 and the Nyquist plots in Fig. 5(b), it was observed that the unmodified carbon felt exhibited the largest overall impedance and the slowest electron transfer kinetics. The semicircular shapes of the curves for all electrodes suggest that charge transfer was predominantly controlled by ohmic polarization. Notably, the WO_3–carbon felt electrode displayed a significantly smaller semicircle, indicating a lower R_{ct} and thus a faster electron transfer rate. This enhancement was attributed to the introduction of WO_3, which improved the electrical conductivity of the carbon felt through increased active sites and improved charge mobility. These results confirm that the hydrothermal modification of carbon felt with WO_3 effectively reduces interfacial resistance and enhances electrochemical performance, making it a promising electrode material for electrochemical applications such as heavy metal recovery from wastewater.

3.2.2.3 Linear sweep voltammetry (LSV). To minimize interference from other ions, the electrolyte solution was prepared using copper(II) sulfate pentahydrate ($CuSO_4 \cdot 5H_2O$) at a concentration of 19 531 mg L^{-1}, corresponding to 5000 mg L^{-1} of Cu^{2+}. The pH of the solution was adjusted to 0.7 using concentrated sulfuric acid. LSV tests were performed using an electrochemical workstation in a three-electrode system, where the hydrothermally synthesized WO_3–carbon felt electrode and the unmodified carbon felt electrode served as working electrodes, Ag/AgCl was used as the reference electrode, and a platinum electrode served as the counter electrode. The potential was scanned from 0 V to 0.6 V at a sweep rate of 5 mV s^{-1}. The results are shown in Fig. 5(c). As illustrated in the LSV curves, both electrode materials exhibited a distinct reduction peak, corresponding to the electrochemical reduction of Cu^{2+} ions in the solution. Notably, the reduction peak for the WO_3–carbon felt electrode appeared at a more positive potential than that for the ordinary carbon felt electrode, indicating that the overpotential required for copper reduction was significantly lower. This suggests that the semiconducting properties of WO_3, when integrated into the carbon felt matrix, synergize with the electrical conductivity of the substrate, thereby facilitating more efficient charge transfer and enhancing the electrode's catalytic activity. Moreover, the current density at the end of the scan was substantially higher for the WO_3–carbon felt electrode than for the unmodified carbon felt electrode. This increase indicated the presence of more electroactive sites on the surface of the WO_3–modified electrode, resulting in faster reaction kinetics.

Table 3 EIS fitting data results of WO_3–carbon felt electrodes

Electrode	R_s (Ω)	R_{ct} (Ω)	W (Ω)
Hydrothermal	1.278	0.14	4.25
Carbon felt	1.69	1.12	13.41

Overall, the LSV results demonstrated that the incorporation of WO_3 significantly enhanced the electrochemical performance of carbon felt electrodes, particularly in terms of conductivity and copper ion reduction efficiency.

3.3 Performance study of WO_3–carbon felt electrode

Optimizing electrolysis operating conditions is critical for enhancing the efficiency of copper ion recovery from wastewater and minimizing energy consumption. In this section, the applied voltage, pH (adjusted by NaOH dosage), and electrolysis duration were systematically varied to evaluate their effects on the performance of the WO_3–carbon felt electrode during the treatment of PCB wastewater.

The goal was to maximize copper removal efficiency and recovery yield while minimizing energy input, thereby improving the overall cost-effectiveness of the process. Optimization of these parameters not only enhanced the electrochemical performance of the WO_3–carbon felt electrode but also laid a solid foundation for its practical application in industrial wastewater treatment.

3.3.1 Effect of pH on electrode performance. To accurately evaluate the influence of initial pH on the electrochemical electrolysis process, Visual MINTEQ software was employed to simulate and predict the speciation of copper ions under varying pH conditions. This approach helped to avoid interference from the formation of copper complexes or precipitates that could adversely affect the electrochemical reduction of Cu^{2+}. The simulation was conducted using a Cu^{2+} concentration of 5000 mg L^{-1} (equivalent to the experimental condition), at a constant temperature of 25 °C, and in the absence of other interfering ions.

According to the Visual MINTEQ simulation results shown in Fig. 6, copper primarily existed as free Cu^{2+} ions in highly acidic environments. However, when the pH increased to around 4, Cu^{2+} began to transform into other species, including copper hydroxide complexes, and may even precipitate from the solution. This phenomenon posed a risk of reducing the availability of electroactive Cu^{2+}, which would negatively affect the electrolysis process. In practical applications, the addition of alkaline agents must be carefully controlled. Excessive NaOH dosage can rapidly elevate the solution pH to near-neutral levels (*e.g.*, approximately pH 7 with 10 g L^{-1} NaOH), resulting in visible turbidity and precipitation, which disrupts the electrochemical reduction process and renders the experiment inoperable.

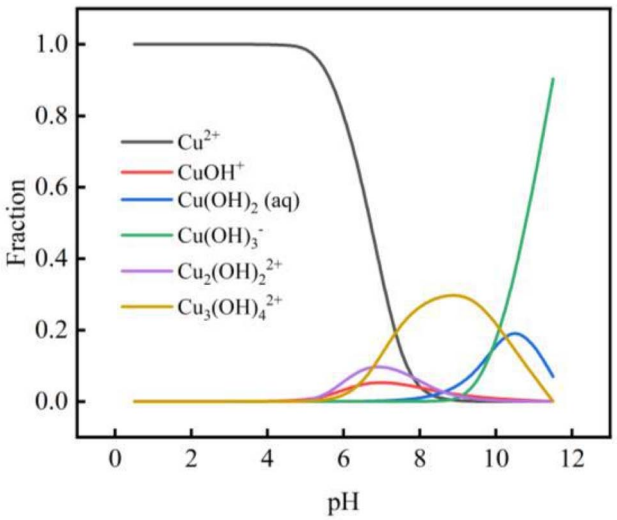

Fig. 6 Existing forms of Cu^{2+} in wastewater under different pH conditions.

To investigate the effect of moderate pH adjustment, simulated PCB wastewater was prepared with NaOH dosages of 0, 3, 6, and 9 g L^{-1}, corresponding to pH values of approximately 0.70, 1.01, 1.35, and 2.01, respectively. Electrolysis experiments were conducted using the hydrothermally prepared WO_3–carbon felt electrode at an applied voltage of 3.0 V, an initial Cu^{2+} concentration of 5000 mg L^{-1}, and an electrolysis time of 5 h.

As shown in Fig. 7(a), moderate additions of NaOH (*i.e.*, avoiding excessive pH rise) led to the steady increase in copper removal efficiency and a corresponding increase in initial current. Specifically, when no NaOH was added (0 g L^{-1}), the removal rate of Cu^{2+} reached 52.8% with an initial current of 0.258 A. With NaOH dosages of 3 g L^{-1} and 6 g L^{-1}, the removal rates improved to 57.2% and 62.9%, respectively. When 9 g L^{-1} of NaOH was added, the removal efficiency further increased to 70.1%, representing an 18.7% enhancement compared to the unadjusted condition. Concurrently, the initial current also rose significantly, reaching 0.339 A. These results indicate that appropriate pH regulation through controlled addition of NaOH can effectively enhance copper removal in the electrochemical electrolysis system by improving both ion availability and reaction kinetics.

The addition of a non-excessive amount of NaOH to simulated PCB wastewater significantly enhanced the efficiency of the electrochemical process. This was attributed to two main factors. First, under strongly acidic conditions with low pH, the high concentration of H^+ ions in the solution led to rapid mass transfer, which induced concentration polarization or electrochemical polarization. As a result, the hydrogen overpotential decreased, increasing the proportion of the hydrogen evolution reaction (HER).[32] As the pH increased, the HER proportion declined, allowing more electrons to be available for Cu^{2+} reduction, thereby improving the removal efficiency of copper. Second, NaOH addition introduced Na^+ ions, which, at moderate levels, enhanced the solution's conductivity and facilitated the reaction. However, excessive NaOH shifts the solution to weakly acidic/alkaline conditions, forming copper hydroxide precipitates. This reduces free Cu^{2+}, re-increases HER, and diminishes electrochemical performance—while also raising reagent costs. Thus, an acidic initial pH is preferred, with 9 g L^{-1} NaOH identified as optimal.

3.3.2 Effect of electrolysis time. Electrochemical treatment of simulated PCB wastewater was conducted under the conditions of an applied voltage of 3.0 V, an initial Cu^{2+} concentration of 5000 mg L^{-1}, and no NaOH addition (0 g L^{-1}). Samples were collected at 3, 4, 5, and 6 hours during the electrolysis process.

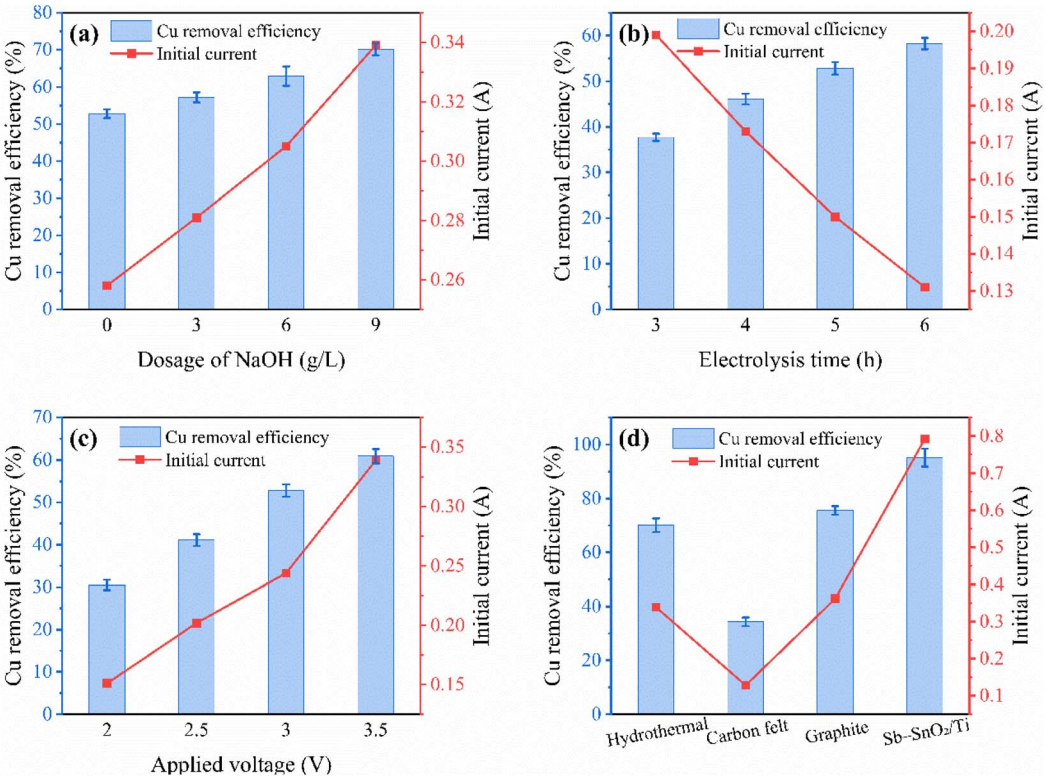

Fig. 7 Cu removal efficiency and the initial current of the WO_3–modified electrode under different (a) NaOH dosage, (b) electrolysis time and (c) applied voltage. (d) Performance comparison of prepared carbon felt electrodes and the electrodes of other materials.

As shown in Fig. 7(b), the WO_3–carbon felt electrode material prepared *via* the hydrothermal method exhibited increasing Cu removal efficiency from simulated PCB wastewater with prolonged electrolysis time. However, the trend of the curve indicated that the rate of increase in Cu removal slowed down over time. Within the first 3 hours, the Cu removal efficiency reached 37.7%, while it increased to 58.2% after 6 hours, indicating that the removal efficiency improved by only 20.5% in the latter 3 hours. This suggests that extending the electrolysis time beyond a certain point yield diminishing returns in Cu removal. Several factors contributed to this phenomenon. On one hand, the composition of the simulated PCB wastewater includes copper sulfate ($CuSO_4$), concentrated sulfuric acid (H_2SO_4), glucose ($C_6H_{12}O_6$), and ammonium sulfate ($(NH_4)_2SO_4$). As electrolysis proceeded, Cu^{2+} ions were reduced and deposited onto the WO_3–carbon felt electrode, leading to a continuous decrease in the ionic concentration of the solution and, consequently, a reduction in conductivity. This resulted in a slower rate of Cu removal. On the other hand, as the Cu^{2+} concentration in the solution decreased, the proportion of the hydrogen evolution reaction (HER) increased. The evolution of hydrogen gas at the cathode not only interfered with the reduction of copper but also impeded the contact between Cu^{2+} ions and active sites on the cathode surface, thus affecting the overall electrochemical process. Moreover, the current intensity during the electrolysis gradually declined. While deposited Cu forms a WO_3–Cu–carbon felt composite (enhancing conductivity *via* metallic copper), the electrolyte's simple composition means falling Cu^{2+} concentrations still reduce overall solution conductivity over time. In addition, the accumulation of copper on the cathode led to a reduction in the number of available active sites. Furthermore, under the influence of the electric field, Cu^{2+} ions continuously migrated toward the cathode, potentially causing local concentration polarization and hindering mass transfer. Due to the combined effects of decreasing current, reduced conductivity, increased HER interference, and limited active sites, the electrochemical process became less efficient over time. Therefore, in practical applications, it was essential to consider the trade-offs between solution conductivity, side reactions, and energy consumption to determine the optimal electrolysis duration through further cost-benefit analysis.

3.3.3 Effect of applied voltage. Electrolysis experiments were conducted on simulated PCB wastewater under applied voltages of 2.0 V, 2.5 V, 3.0 V, and 3.5 V, with an initial Cu^{2+} concentration of 5000 mg L^{-1} and no NaOH addition (0 g L^{-1}). As shown in Fig. 7(c), the Cu removal efficiency of the WO_3–carbon felt electrode under four different applied voltages increased with the rise in voltage. When the applied voltage was increased from 2.0 V to 3.5 V, the Cu removal efficiencies after 5 hours were 30.5%, 41.1%, 52.8%, and 60.9%, respectively. A closer examination revealed that the improvement in Cu removal efficiency from 3.0 V to 3.5 V was less significant than the increase observed from 2.5 V to 3.0 V. This was attributed to the typical behavior of electrochemical systems under increasing voltage, which generally progresses through three stages. In the low-voltage region, the

current increased exponentially with the applied voltage, leading to a significant improvement in Cu removal. In the medium-voltage region, the rate of current increase slowed down. In the high-voltage region, the current began to saturate as the diffusion rate of Cu^{2+} became limited and side reactions, such as water decomposition, became more pronounced, thereby reducing the rate of current increase. Notably, when the applied voltage was raised to 4.0 V, visible gas bubbles were observed on the cathode, indicating that the hydrogen evolution reaction (HER) significantly interfered with the electrolysis process. The escape of gas bubbles not only hindered the reduction and deposition of copper but also dislodged WO_3 particles from the carbon felt, compromising the electrode's stability and lifespan. Therefore, to avoid such issues and to balance energy consumption in practical applications, the applied voltage should be carefully controlled. In this study, 3.0 V was identified as the optimal applied voltage.

3.3.4 Orthogonal experimental design. The electrochemical removal efficiency of copper from simulated PCB wastewater was used as the evaluation metric. Based on preliminary experiments and the underlying principles, three key factors were identified: electrolysis time (3, 4, 5, and 6 hours), NaOH dosage (0, 3, 6, and 9 g L^{-1}), and applied voltage (2.0, 2.5, 3.0, and 3.5 V). An orthogonal experimental design and range analysis of the results were performed using SPSS software. The orthogonal experiment results for the hydrothermally prepared WO_3–carbon felt electrode were summarized in Table 4.

Range analysis was performed on the orthogonal experimental data, where the value R represented the range and directly reflected the influence of each factor. A larger R value indicated a greater impact on the experimental outcome. The final evaluation metric for this experiment was the Cu removal efficiency from PCB wastewater using different electrodes under various operating conditions. The range analysis results were summarized in Table 5. The K values represented the average of the experimental data corresponding to each level of a given factor. Specifically, K_1, K_2, K_3, and K_4 corresponded to different levels of the factor (for example, K_1 corresponded to 0 g L^{-1} NaOH dosage, 2.0 V applied voltage, and 3 h electrolysis time).

Table 4 Summary of orthogonal experiment data of PCB wastewater treatment with WO_3–carbon felt electrode prepared by the hydrothermal method

Run	Dosage of NaOH (g L^{-1})	Applied voltage (V)	Electrolysis time (h)	Cu removal rate (%)
1	0	2.0	3	19.6
2	0	2.5	4	34.0
3	0	3.0	5	52.8
4	0	3.5	6	68.7
5	3	2.0	4	28.8
6	3	2.5	3	29.1
7	3	3.0	6	63.5
8	3	3.5	5	65.6
9	6	2.0	5	38.3
10	6	2.5	6	53.8
11	6	3.0	3	39.4
12	6	3.5	4	59.7
13	9	2.0	6	47.1
14	9	2.5	5	52.6
15	9	3.0	4	60.8
16	9	3.5	3	50.4

Table 5 Range analysis

	Dosage of NaOH	Applied voltage	Electrolysis time
K_1	43.78	33.45	34.63
K_2	46.75	42.38	45.83
K_3	47.80	54.13	52.32
K_4	52.73	61.10	58.27
R	8.95	27.65	23.65

Based on Table 5, the following conclusions were drawn: considering individual factors, increasing the NaOH dosage from 0 to 3 g L^{-1} resulted in a noticeable improvement in Cu removal efficiency, while the increase from 6 to 9 g L^{-1} contributed significantly more. However, the contribution from 3 to 6 g L^{-1} was relatively minor. Regarding the applied voltage, its increase consistently led to a marked enhancement in Cu removal efficiency. Nevertheless, a decrease in slope was shown when the voltage rose from 3.0 V to 3.5 V, indicating a limitation in the improvement effect. The effect of electrolysis time exhibited a less pronounced arch-shaped trend in the R values, suggesting that the relationship between electrolysis time and Cu removal was not linear.

Considering all factors, the average R values were 27.65 for applied voltage, 23.65 for electrolysis time, and 8.95 for NaOH dosage. This indicated the order of significance on Cu removal efficiency as: applied voltage > electrolysis time > NaOH dosage. Therefore, the optimal operating conditions were determined as an applied voltage of 3.0 V, an electrolysis time of 5 hours, and a NaOH dosage of 9 g L^{-1}.

3.3.5 Comparison of WO_3–carbon felt with other materials. To evaluate the practical application potential of the WO_3–carbon felt electrode, its performance was compared with that of the bare carbon felt electrode substrate, the commonly used commercial graphite electrode, and the tin–antimony titanium (Sn–Sb/Ti) electrode. The graphite electrode and Sn–Sb/Ti electrode was purchased from Superior Electronic Materials Trading Co. (Suzhou, China). Based on the orthogonal experimental results, the test conditions were set as an applied voltage of 3.0 V, electrolysis time of 5 hours, and NaOH dosage of 9 g L^{-1}. As shown in Fig. 7(d), under the conditions of 3.0 V applied voltage, 5 hours electrolysis time, and 9 g L^{-1} NaOH dosage, the WO_3–carbon felt electrode prepared *via* the hydrothermal method achieved a Cu removal efficiency of 70.1% from wastewater. This was significantly higher than that of the bare carbon felt electrode (34.3%), slightly lower than the graphite plate electrode (75.6%), while the tin–antimony titanium (Sn–Sb/Ti) electrode exceeded 90% Cu removal after only 3 hours of electrolysis and stopped the process at approximately 210 minutes, reaching 95.1% removal.

The initial current values also indicated that the WO_3–carbon felt electrode exhibits a current magnitude close to that

of the graphite electrode, demonstrating comparable electrochemical performance, both of which were significantly better than that of the bare carbon felt electrode. Overall, these results showed that the hydrothermally prepared WO_3–carbon felt electrode performs far better than ordinary carbon felt and approached the performance of commonly used graphite electrodes. The Sn–Sb/Ti electrode, being a metallic composite material, showed superior performance compared to the other electrodes.

However, considering practical cost factors, a graphite electrode plate sized 50 × 120 × 1 mm cost approximately 4.2 USD, a 50 × 100 × 1 mm Sn–Sb/Ti electrode with a Sn and Sb loading of 10 g m^{-2} costs about 72.2 USD, whereas carbon felt measuring 200 × 1230 × 3 mm was priced at only 6.1 USD. This cost-performance comparison further supported the practical application potential of the hydrothermally prepared WO_3–carbon felt electrode. The calculated cost per unit area of electrode materials revealed substantial differences between the three tested electrode types. The hydrothermally prepared WO_3–carbon felt exhibited the lowest unit-area cost at 24.8 USD m^{-2}, followed by the commercial graphite plate at 694.4 USD m^{-2}, while the Sn–Sb/Ti electrode presented an exceptionally high cost of 14 444 USD m^{-2}. This variation of more than two orders of magnitude indicates that electrode material selection has a decisive impact on the economic feasibility of large-scale implementation. Above cost price of the above raw materials is based on our actual purchase prices from suppliers. Industrial bulk purchases may yield lower prices.

3.3.6 Reusability of WO_3–carbon felt electrode. Continuous electrolysis experiments were conducted to evaluate the stability of the WO_3–carbon felt electrode prepared *via* the hydrothermal method. The applied voltage was set to 3.0 V, NaOH dosage was set to 9 g L^{-1}, and electrolysis time was set to 5 hours. Four consecutive electrolysis cycles were performed. After each cycle, the WO_3–carbon felt electrode was cleaned and scraped to remove the deposited copper from its surface.

As shown in Fig. 8, in the first electrolysis cycle, the electrode achieved a Cu removal efficiency of 70.1%, indicating excellent electrochemical performance. However, after consecutive electrolysis cycles, the removal efficiency decreased to 64.5% in the second cycle and further declined to 57.2% in the third cycle. This gradual performance degradation may be attributed to the detachment of WO_3 from the carbon felt surface during electrolysis due to the applied voltage and continuous stirring, or to corrosion caused by the highly acidic electrolyte and high concentrations of heavy metals. In the fourth cycle, the Cu removal efficiency further dropped to 51.6%. Nevertheless, the performance remained significantly higher than that of bare carbon felt, demonstrating that despite the impact of hydraulic forces, voltage stress, and electrolyte corrosion, the hydrothermally prepared WO_3–carbon felt electrode maintained a notable performance enhancement. This stability suggested the potential industrial applicability of the material, although further modifications or optimization of electrolysis conditions might be necessary to improve its durability under continuous operation. Overall, although a certain degree of performance decline was observed during the treatment of PCB wastewater, the hydrothermal WO_3–carbon felt electrode still outperformed the ordinary carbon felt electrode, indicating promising application prospects. Future research should focus on enhancing the stability of the material under repeated use to meet industrial requirements.

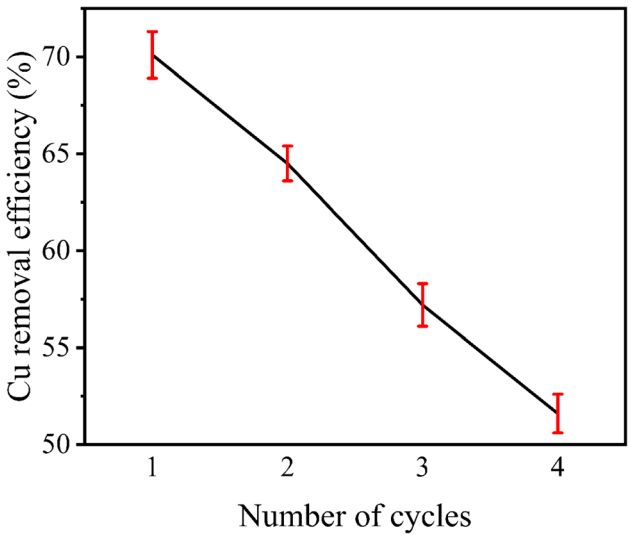

Fig. 8 Study on continuous electrolysis stability of copper in PCB wastewater treated by WO_3–carbon felt electrode.

In summary, the WO_3 powder in the hydrothermal WO_3–carbon felt electrode possesses a nanostructure with a high specific surface area, providing more active sites during electrolysis and thus better initial performance. However, since the coating method relies on physical adsorption, WO_3 can easily detach during operation, leading to significant performance degradation. Therefore, further studies are needed to address these limitations in practical applications, depending on specific conditions.

3.3.7 Effect of COD on the electrochemical performance. Under the optimal experimental conditions, the WO_3–carbon felt electrode prepared *via* the hydrothermal method achieved a Cu removal efficiency of 70.1% from wastewater. Compared to other literature reports, this value was relatively low. This discrepancy was likely because other studies typically used simple copper sulfate solutions without high COD content,[33–35] whereas the simulated wastewater in this study contained 1000 mg L^{-1} COD, better reflecting real wastewater conditions, which led to a lower Cu removal efficiency. Additionally, the simulated wastewater in this study also contained a certain amount of ammonia nitrogen (NH_4^+–N, 20 mg L^{-1}). It has been shown that formation of the tetraamminecopper(II) complex in ammonia-containing solutions shifts the Cu(II)/Cu(I) and Cu(II)/Cu^0 reduction potential to more positive values, making reduction thermodynamically less favourable under the same applied potential.[36] However, due to its low concentration, the impact was minor. To investigate the effect of COD on Cu removal during electrolysis, experiments were conducted using simulated wastewater without COD.

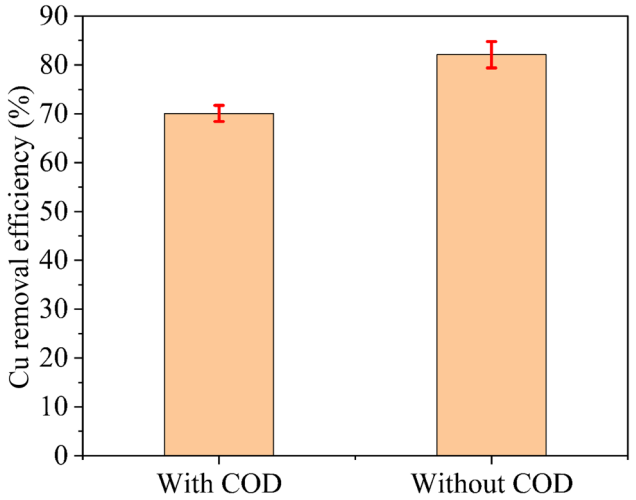

Fig. 9 The impact of COD on the electrodes.

In the electrolysis experiments using simulated PCB wastewater containing COD, samples were taken and analyzed before and after electrolysis. The COD concentration decreased from 983.6 mg L^{-1} before electrolysis to 653.4 mg L^{-1} after electrolysis, corresponding to a removal rate of 33.6%. When electrolysis was performed on simulated PCB wastewater without added COD, the Cu removal efficiency of the hydrothermally prepared WO_3–carbon felt electrode increased to 82.1%, an improvement of over 10% (Fig. 9). It was evident that COD in the wastewater affected the actual electrolysis performance. During the electrolysis of COD-containing wastewater, organic substances such as glucose were oxidized at the anode into CO_2 and other products. This oxidation consumed part of the current, thereby reducing the effective current available for copper reduction. Moreover, literature reports indicated that oxygen reduction reactions occurred during electrolysis, producing species such as H_2O_2 and hydroxyl radicals (·OH).[37] The formation of H_2O_2 was attributed to different valence states of copper ions generated under the electric field *via* a Fenton-like process.[38] Additionally, the catalytic effects of WO_3 and Cu/Cu_2O on the cathode surface could also generate strong oxidants like hydroxyl radicals.[39] These processes contributed to the decrease of COD in the wastewater but also affected the current fraction for copper deposition and hinder mass transfer, resulting in a reduction in Cu removal efficiency. Therefore, in practical electrolysis applications, pretreatment to reduce COD levels in wastewater should be considered.

3.4 Mechanism of Cu removal

Through electrolysis, copper ions in water were reduced to solid copper metal for recovery. The reduction of Cu^{2+} ions during electrolysis proceeds primarily through the two-electron reaction. Under less cathodic potentials, Cu^{2+} may be incompletely reduced, forming cupric oxide. On the WO_3–carbon felt electrode, the reduction process was facilitated by the reversible redox transition of tungsten oxide.[40] The relevant chemical equations are as follows:

$$Cu^{2+} + 2e^- \rightarrow Cu(s)$$

$$2Cu^{2+} + H_2O + 2e^- \rightarrow Cu_2O(s) + 2H^+$$

$$WO_3 + xH^+ + xe^- \rightleftharpoons H_xWO_3$$

The formation of H_xWO_3 enhances the local electronic conductivity and creates transient electron–proton storage sites that assist the charge transfer to Cu^{2+}.[41] As a result, the WO_3–carbon felt exhibits both a catalytic effect, by mediating electron transfer *via* the W^{6+}/W^{5+} couple, and a structural effect, by increasing electroactive surface area and Cu^{2+} adsorption affinity. This dual role lowers the charge-transfer resistance (R_{ct}) and overpotential for Cu^{2+} reduction, consistent with the EIS and LSV results. The overall process can be regarded as a synergistic combination of redox mediation and physical enhancement at the WO_3-modified interface.

4 Perspective

The results of this study demonstrate that hydrothermally prepared WO_3–carbon felt electrodes exhibit high potential for application in the electrolytic recovery of copper from PCB wastewater, offering both enhanced electrochemical performance and economic feasibility. The improvement in catalytic activity, electron transfer efficiency, and removal performance achieved through WO_3 modification confirms the effectiveness of targeted electrode surface engineering for wastewater treatment applications. Although the present work focuses on copper recovery, the design concept and optimization strategy could be extended to the selective recovery of other heavy and valuable metals frequently present in electronic waste streams, including nickel, cobalt, and precious metals, through appropriate adjustment of electrode composition and operating parameters.

Optimizing key operational factors (applied voltage, NaOH dosage, and electrolysis time) was critical for balancing removal efficiency, energy consumption, and material stability. The orthogonal design provides a systematic approach to adapt to variable industrial wastewater compositions, offering a practical framework for process scale-up. While the WO_3–carbon felt electrodes achieved performance comparable to that of commercial graphite electrodes at substantially lower material cost, the observed decrease in removal efficiency during repeated cycles indicates that electrode stability remains a primary limitation. Improving WO_3 adhesion to carbon felt (*e.g.*, *via* chemical bonding or composite binders) and optimizing regeneration protocols can significantly boost long-term operational stability.

In addition, the inhibitory influence of high COD on copper removal efficiency observed in this study highlights the necessity of integrating electrochemical recovery with appropriate pretreatment measures, such as advanced oxidation or adsorption processes, to reduce organic load prior to electrolysis. This integration would be expected to improve both

recovery efficiency and process robustness under actual wastewater conditions.

From a broader perspective, the development of low-cost, high-performance electrode materials aligns with the principles of sustainable resource recovery and circular economy, providing a viable route for the simultaneous reduction of environmental impact and reclamation of critical metal resources. Continued efforts in electrode material innovation, system integration, and stability enhancement will be essential to advance this technology from laboratory-scale validation toward industrial-scale implementation.

5 Conclusion

This work developed high-performance WO_3–carbon felt electrodes *via* a simple one-step hydrothermal method and applied them to the treatment of PCB wastewater. The optimized electrode achieved a copper removal efficiency of 70.1% under practical conditions, significantly outperforming unmodified carbon felt and approaching the efficiency of commercial graphite electrodes at a fraction of the cost. Orthogonal experiments identified applied voltage as the most influential factor, followed by electrolysis time and NaOH dosage. Cost-performance analysis confirmed the outstanding economic advantage of WO_3–carbon felt compared with conventional electrode materials, reinforcing its potential for large-scale application. Although repeated use led to partial WO_3 detachment and efficiency loss, the electrode consistently outperformed bare carbon felt, indicating good reusability. Overall, the hydrothermal WO_3–carbon felt electrode provides a sustainable, cost-effective, and scalable pathway for electrolytic copper recovery, with promising prospects for integration into industrial wastewater treatment and extension to other valuable or toxic metals.

Conflicts of interest

There are no conflicts to declare.

Data availability

The data supporting this article have been included as part of the supplementary information (SI). Supplementary information: additional characterization data and supporting electrochemical measurements. See DOI: https://doi.org/10.1039/d5ra07199b.

References

1 Y. Xue and Y. Wang, *Green Chem.*, 2020, **22**, 6288–6309.
2 I. M. S. K. Ilankoon, Y. Ghorbani, M. N. Chong, G. Herath, T. Moyo and J. Petersen, *Waste Manag.*, 2018, **82**, 258–275.
3 M. A. Fathy, S. M. Abdelbasir, S. S. Hassan, A. H. Kamel and D. Rayan, *J. Mater. Cycles Waste Manag.*, 2021, **23**, 1090–1101.
4 B. Ghosh, M. K. Ghosh, P. Parhi, P. S. Mukherjee and B. K. Mishra, *J. Clean. Prod.*, 2015, **94**, 5–19.
5 F. Jiang, X. Xu, X. Feng, M. Wang, C. Zhang, Y. Mao, M. Xing, P. Li, Q. Han, H. Pan, J. Wang and M. Wang, *J. Hazard. Mater.*, 2025, **497**, 139613.
6 E. Blumbergs, A. Shishkin, K. Markus, V. Serga, D. Goljandin, A. Klauson, V. Abramovskis, J. Baronins, A. Zarkov and V. Pankratov, *Metals*, 2024, **14**, 95.
7 L. Sun, X. Zeng, and J. Li, ed. J. Li and F. Dong, *Selected Proceedings of the Tenth International Conference on Waste Management and Technology*, 2016, vol. 31, pp. 867–872.
8 J. Cui and L. Zhang, *J. Hazard Mater.*, 2008, **158**, 228–256.
9 S. Krishnan, N. S. Zulkapli, H. Kamyab, S. M. Taib, M. F. B. M. Din, Z. Abd Majid, S. Chaiprapat, I. Kenzo, Y. Ichikawa, M. Nasrullah, S. Chelliapan and N. Othman, *Environ. Technol. Innovat.*, 2021, **22**, 101525.
10 E. Hsu, K. Barmak, A. C. West and A.-H. A. Park, *Green Chem.*, 2019, **21**, 919–936.
11 H. Li, J. Eksteen and E. Oraby, *Resour. Conserv. Recycl.*, 2018, **139**, 122–139.
12 S. Jadoun, S. Chinnam, S. Jabin, Y. Upadhyay, N. K. Jangid and J. Zia, *Environ. Sci. Technol. Lett.*, 2024, **12**, 8–24.
13 Y. Liu, Y.-Y. Deng, Q. Zhang and H. Liu, *Sci. Total Environ.*, 2021, **757**, 143901.
14 H. I. Maarof, W. M. A. W. Daud and M. K. Aroua, *Rev. Chem. Eng.*, 2017, **33**, 359–386.
15 P. Srimuk, X. Su, J. Yoon, D. Aurbach and V. Presser, *Nat. Rev. Mater.*, 2020, **5**, 517–538.
16 Y. Feng, L. Yang, J. Liu and B. E. Logan, *Environ. Sci.:Water Res. Technol.*, 2016, **2**, 800–831.
17 E. Bazrafshan, L. Mohammadi, A. Ansari-Moghaddam and A. H. Mahvi, *J. Environ. Health Sci. Eng.*, 2015, **13**, 74.
18 M. Li, N. Chen, H. Shang, C. Ling, K. Wei, S. Zhao, B. Zhou, F. Jia, Z. Ai and L. Zhang, *Environ. Sci. Technol.*, 2022, **56**, 10945–10953.
19 S. S. M. Hassan and M. A. Fathy, *Microchim. Acta*, 2024, **191**, 427.
20 W. Chen, M. Li and J. Tang, *Metals*, 2023, **13**, 643.
21 A. Kuleyin and H. E. Uysal, *Int. J. Electrochem. Sci.*, 2020, **15**, 1474–1485.
22 Y. Liu, H. Wang, Y. Cui and N. Chen, *Int. J. Environ. Res. Publ. Health*, 2023, **20**, 3885.
23 G. A. Tonini and L. A. Martins Ruotolo, *Clean Technol. Environ. Policy*, 2017, **19**, 403–415.
24 H. C. Gulyasar, *Water Air Soil Pollut.*, 2025, **236**, 327.
25 J. Lee, G. Antonini, A. Al-Omari, C. Muller, J. Mathew, K. Bell, J. M. Pearce and D. Santoro, *Sustainability*, 2024, **16**, 9764.
26 L. Yang, W. Hu, Z. Chang, T. Liu, D. Fang, P. Shao, H. Shi and X. Luo, *Environ. Int.*, 2021, **152**, 106512.
27 F. Mashkoor, D. Kim, M. Z. Ansari, A. H. Anwer, M. Shoeb and C. Jeong, *J. Mol. Liq.*, 2023, **375**, 121312.
28 J. Sun, L. Liu and F. Yang, *J. Hazard Mater.*, 2020, **394**, 122534.
29 Y. Zhang, C. You, M. Ren, M. Liu, X. Xu, Y. Zhang, A. Lin, Y. Pei, D. Yuan and J. Cui, *J. Hazard Mater.*, 2022, **429**, 128352.
30 N. M. Shinde, A. D. Jagadale, V. S. Kumbhar, T. R. Rana, J. Kim and C. D. Lokhande, *Kor. J. Chem. Eng.*, 2015, **32**, 974–979.

31 L. Shen, L. Du, S. Tan, Z. Zang, C. Zhao and W. Mai, *Chem. Commun.*, 2016, **52**, 6296–6299.
32 T. C. d. M. Nepel, J. M. Costa, M. G. A. Vieira and A. F. de Almeida Neto, *Environ. Technol.*, 2022, **43**, 469–477.
33 S. Chellammal, S. Raghu, P. Kalaiselvi and G. Subramanian, *J. Hazard Mater.*, 2010, **180**, 91–97.
34 T. R. Da Silva, D. Majuste, J. Bauer and M. S. Moats, *Hydrometallurgy*, 2020, **198**, 105513.
35 Y. Delgado, F. J. Fernandez-Morales and J. Llanos, *Molecules*, 2021, **26**, 5525.
36 P. Lin, J. Werner, Z. A. Ali, L. Bertucci and J. Groppo, *Materials*, 2023, **16**, 6274.
37 W. Zhou, X. Meng, J. Gao and A. N. Alshawabkeh, *Chemosphere*, 2019, **225**, 588–607.
38 Z. Ai, H. Xiao, T. Mei, J. Liu, L. Zhang, K. Deng and J. Qiu, *J. Phys. Chem. C*, 2008, **112**, 11929–11935.
39 X. Mi, J. Han, Y. Sun, Y. Li, W. Hu and S. Zhan, *J. Hazard Mater.*, 2019, **367**, 365–374.
40 B. Ma, E. W. Huang, G. J. Wu, W. L. Dai, N. J. Guan and L. D. Li, *RSC Adv.*, 2017, **7**, 2606–2614.
41 R. Matsuo, T. Yamasaki and T. Omata, *J. Mater. Chem. A*, 2025, **13**, 40131–40138.